Relativistic Computational Investigation: The Geometries and Electronic Properties of $TaSi_n^+$ ($n = 1-13, 16$) Clusters

Ping Guo,[†,‡] Zhao-Yu Ren,[*,†] A-Ping Yang,[†] Ju-Guang Han,[*,§] Jiang Bian,[||] and Guang-Hou Wang[⊥]

Institute of Photonics & Photon-Technology and Department of Physics, Northwest University, Xi'an 710069, China, Department of Chemistry and Biochemistry, Montana State University, Montana 59715, State Key Laboratory of Rare Earth Materials Chemistry and Applications, College of Chemistry and Molecular Engineering, Peking University, Beijing 100871, China, and Key Laboratory of Solid-State Microstructures, Nanjing University, Nanjing 210093, China

Received: January 8, 2006; In Final Form: April 13, 2006

The equilibrium geometries, stabilities, and electronic properties of the $TaSi_n^+$ ($n = 1-13, 16$) clusters are investigated systematically by using the relativistic density functional method with generalized gradient approximation. The small-sized $TaSi_n^+$ clusters with slight geometrical adjustments basically keep the frameworks that are analogous to the neutrals while the medium-sized charged clusters significantly deform the neutral geometries, which are confirmed by the calculated AIP and VIP values. Furthermore, the optimized geometries of the charged clusters agree with the experimental results of Hiura and co-workers (Hiura, H.; Miyazaki, T.; Kanayama, T. *Phys. Rev. Lett.* **2001**, *86*, 1733). The highest occupied molecular orbital (HOMO) and lowest unoccupied molecular orbital (LUMO) gaps of the charged clusters are generally increased as the cluster size goes from $n = 1$ to 13; and the large HOMO−LUMO gaps of charged clusters resulting from the positive charge indicate that their chemical stabilities are stronger than their neutral counterparts, especially for $n = 4$, 6, and 7 clusters. Additionally, the contributions of the d orbitals of the Ta atom to the HOMO and LUMO reveal that the chemical activity of the d orbitals of the Ta atom decreases gradually as the number of silicon atoms increases. This interesting finding is in good agreement with the recent experimental results on the reactive activities of the H_2O and transition-metal silicon clusters (Koyasu, K.; Akutsu, M.; Mitsui, M.; Nakajima, A. *J. Am. Chem. Soc*. **2005**, *127*, 4998). Generally, the positive charge significantly influences the electronic and geometric structures of the charged clusters. Finally, the most stable neutral and charged $TaSi_{16}$ clusters are found to be fullerene-like structures and the HOMO−LUMO gap in charged form is detectable experimentally.

1. Introduction

Fabrication of cluster-assembled materials depends on finding suitable building blocks for a cluster that are chemically stable and interact weakly with each other.[1] Because silicon is a semiconducting element of great importance in the microelectronics industry, the Si_n clusters had been investigated extensively both experimentally and theoretically.[2−12] Moreover, the pure silicon clusters are chemically reactive because of the universal existence of dangling bonds (DBs)[10−12] and thus unsuitable as the building blocks of self-assembly materials. This motivates a search for a way to stabilize Si_n cagelike clusters, and inserting a transition-metal atom into the Si_n clusters has changed the status dramatically. Compared with the pure silicon clusters, transition-metal-doped silicon clusters have enhanced stability, exhibiting a strong size selectively and large gap between the highest occupied molecular orbital and the lowest unoccupied molecular orbital (HOMO−LUMO) gap. Thus, they can ensure the chemical stability of a cluster and form the building blocks for cluster-assembled materials, so it should be possible to develop silicon-based devices for various optoelectronic applications by assembling them properly.[13−17] Since Beck[18,19] and Hiura[20] produced transition-metal-doped silicon clusters, a number of computational investigations were performed on the transition-metal-doped silicon clusters.[21−34] It has been shown recently that the respective semiconducting and metallic properties of these clusters could lead to an entirely new range of silicon-based applications in optoelectronic and other devices.

Stimulated by Hiura's experimental findings, the computational investigations of the equilibrium geometries, stabilities, and electronic properties of the neutral $TaSi_n$ ($n = 1-13$) clusters with various spin configurations were carried out by using the relativistic density function theory (RDFT) method.[32] Calculated results indicated that the most stable $TaSi_n$ ($n = 1-6$) clusters keep the analogous frameworks as the most stable Si_{n+1} clusters except for $TaSi_3$ and that the Ta atom in the lowest-energy $TaSi_n$ ($n = 1-11$) isomers occupies a gradual sinking surface site while the Ta atom in $TaSi_{12}$ cluster is completely encapsulated into the center site of the Si_{12} frame and a stable cagelike $TaSi_{12}$ geometry is formed. However, the investigations on fragmentation energies show that the $TaSi_n$ ($n = 2$, 3, 5, 7,

* To whom correspondence should be addressed. Address: Institute of Photonics & Photon-Technology, Northwest University, Xi'an, 710069, China. Fax: +86-29-88303336. E-mail: jghan@ustc.edu.cn; rzy@nwu.edu.cn.
[†] Institute of Photonics & Photon-Technology, Northwest University.
[‡] Department of Physics, Northwest University.
[§] Montana State University.
[||] Peking University.
[⊥] Nanjing University.

10.1021/jp060130f CCC: $33.50
Published on Web 05/20/2006

10, 11, 12) clusters have enhanced thermodynamic stabilities. Theoretical results on the small neutral clusters cannot give the excellent interpretations of Hiura's experimental results, which show the $TaSi_n^+$ ($n = 4, 6, 8, 9, 11, 12$) clusters having enhanced stabilities, or exhibit the abundant isomers. On the basis of the comparison above and the fact that the $TaSi_n^+$ clusters are experimentally detected as ions, we speculated that the influences of the positive charge on the small-sized $TaSi_n$ geometries are significant. For the large-sized $TaSi_n$ ($n \geq 12$) clusters, although the initial transition-metal atom is ionized positively, the positive charge would be spread within the whole cluster after the transitional metal is encapsulated into the Si_n cages. As a rough estimation on the influence of the positive charge, the geometrical adjustments are likely to be larger for the small-sized clusters than for the large-sized ones. To give a reasonable and accurate interpretation of the influence of the positive charge to the $TaSi_n$ clusters, we performed a detailed study of the $TaSi_n^+$ ($n = 1-13, 16$) clusters and the influences of positive charge on the electronic structures and properties of the $TaSi_n$ clusters by using the relativistic density functional method with a generalized gradient approximation. The considered initial geometries of the charged clusters are obtained from the neutral $TaSi_n$ clusters in our previous work,[32] in which all of the possible $TaSi_n$ isomers with various spin multiplicities are calculated and the lowest-energy $TaSi_n$ clusters are found as a spin doublet state except for the TaSi and $TaSi_2$ with quartet spin configurations. Simultaneously, the fragmentation energies, the HOMO−LUMO gaps, the vertical ionization potentials (VIPs), and the adiabatic ionization potentials (AIPs) are calculated, and the corresponding results are compared with the neutral $TaSi_n$ clusters.[35−36]

2. Computational Details

All geometries and properties are calculated utilizing the ADF program,[37−39] which can perform the density functional theory (DFT) calculations of the small molecules and clusters and implement the self-consistent solution of the Kohn−Sham equations in the local density approximation (LDA),[40] via projection in a Slater-type basis set. To surmount computational task, a frozen-core triple-ζ basis set plus polarization function is employed for the $TaSi_n^+$ clusters. For tantalum and silicon atoms, the inter-shell orbitals are, respectively, kept frozen up to 4d and 2p orbitals. Furthermore, the relativistic calculations are of importance because the $TaSi_n^+$ clusters bear a heavy element (Ta), so a combined scalar relativistic ZORA[37,38] has been considered during geometry optimization. Except for the above explicitly stated, all of the calculations are done based upon the LDA augmented with gradient exchange Becke[41] functionals and Perdew[42] correlation functionals. For each $TaSi_n^+$ cluster, the stability is attested by the harmonic vibrational frequencies. If an imaginary frequency is found, then a relaxation along the coordinates of the imaginary vibrational mode is carried out until a true local minimum is reached.

Although the tests of our calculations have been checked by analyzing bond lengths, vibrational frequencies, and dissociation energies of the Si_2, TaO, TaO^+, and Ta_4 molecules, a good agreement with the available experimental data is found.[32] The bond lengths, atomic averaged binding energies, and lowest harmonic vibrational frequencies of the Si_2, Si_3, Si_7, Ta_4, TaC, and TaC^+ molecules are calculated and listed in Table 1 for further evidences, which are in good agreement with available experimental and theoretical results,[43−47] indicating that our calculations are reliable and accurate, which will provide reliable data of the $TaSi_n^+$ ($n = 1-13, 16$) clusters.

TABLE 1: Bond Length (*R*), Atomic Averaged Binding Energy (*BE*/atom), and the Lowest Harmonic Vibrational Frequency (freq) for the Ground State of the Following Molecules

molecule	method	symmetry	state	*BE*/atom (eV)	*R* (Å)	freq (cm^{-1})
Si_2	ADF	$D_{\infty h}$	$^3\Sigma_g^-$	1.65(0)	2.306	463.50
	EXP[a]		$^3\Sigma_g^-$	1.61(3)	2.246	510.98
Si_3	ADF	D_{3h}	$^3E'$	2.43(0)	2.312	300.7
	EXP[b]	C_{2v}	$^1A_1$	2.45(3)		523.1
Si_7	ADF	D_{5h}	A'_1	3.40(1)	2.502	165.0
	EXP[c]	D_{5h}	A'_1	3.60(6)		345.0
Ta_4	ADF	T_d	$^1A_1$	4.26(0)	2.563	137.6
	EXP[d]	distorted T_d	$^1A_1$			130.6
TaC	ADF	C_{2v}	$^2\Sigma^+$	2.89(0)	1.754	893.9
	CASMCSCF[e]	C_{2v}	$^2\Sigma^+$		1.799	748
TaC^+	ADF	C_{2v}	$^1\Sigma^+$		1.684	1125.2
	CASMCSCF[e]	C_{2v}	$^1\Sigma^+$		1.706	1307

[a] Reference 43. [b] Reference 44. [c] Reference 45. [d] Reference 46. [e] Reference 47.

3. Results and Discussions

3.1. Geometries and Stabilities. The equilibrium geometries of the $TaSi_n$ and $TaSi_n^+$($n = 2-13, 16$) clusters are displayed in Figure 1, in which the cutoff distances of the Ta−Si and the Si−Si bonds are defined as 2.96 and 2.70 Å, respectively. Different $TaSi_n$ and $TaSi_n^+$ isomers are signed additionally by a, b, c, and so on. The total bonding energies, point-group symmetries, electronic states, vibration frequencies, and some bond lengths of the $TaSi_n^+$ ($n = 1-13, 16$) clusters are listed in Table 2, *n*a, *n*b, and *n*c correspond to the $TaSi_n$(a), $TaSi_n$(b), and $TaSi_n$(c) geometries, and *n* is the number of the Si atoms; the additional (+) labels the charged $TaSi_n^+$ clusters.

$TaSi^+$. The electronic state of the C_{2v} $TaSi^+$ clusters is calculated. The triplet $TaSi^+$ cluster is optimized to be ground state with the electronic configuration predicted as $(1a_2)^2(4b_2)^2(7a_1\alpha)^1(4b_1\alpha)^1$, which is different from the most stable quartet TaSi dimer ($(1a_2)^2(4b_1)^2(7a_1\alpha)^1(4b_2\alpha)^1$), and the corresponding electronic state is $^3\Phi$ or $^3\Pi$. On the basis of the calculated population analyses, it obviously indicates that the additional charge is removed from the Ta atom of the triplet $TaSi^+$ cluster, reflecting that the additional charge in the $TaSi^+$ cluster plays an important role in geometry and electronic properties.

The Ta−Si bond length (2.380 Å) in the triplet $TaSi^+$ cluster is slightly longer than that (2.357 Å) of the TaSi cluster, and it is significantly longer than the Ta−C bond length of the TaC^+ (1.731 Å).[47] The atomic averaged binding energies (1.860 eV/atom) of the $TaSi^+$ cluster is higher than that (1.664 eV/atom) of the TaSi cluster. Specifically, the HOMO and LUMO energies of the $TaSi^+$ cluster are lower while the corresponding HOMO−LUMO gap is larger than that of the TaSi cluster, implying that the $TaSi^+$ cluster is a chemically stable structure. These findings indicate that the $TaSi^+$ cluster is more stable than the neutral.

$TaSi_2^+$. On the basis of the neutral $TaSi_2$ isomers,[32] two typical $TaSi_2^+$ structures (the planar 2a(+) and the linear 2b(+)) are considered. The Ta−Si bond lengths and the SiTaSi bond angles of two geometries are similar to those of the neutrals, which are in good agreement with the slight variation in the calculated bonding energy of the above charged clusters. The most stable C_s $TaSi_2^+$ 2a(+) structure is described as the triangular form, and the predicted ground electronic state is $^3A''$. According to the calculated populations, one finds that the positive charge in the $TaSi_2^+$ structures is distributed on the Ta atom.

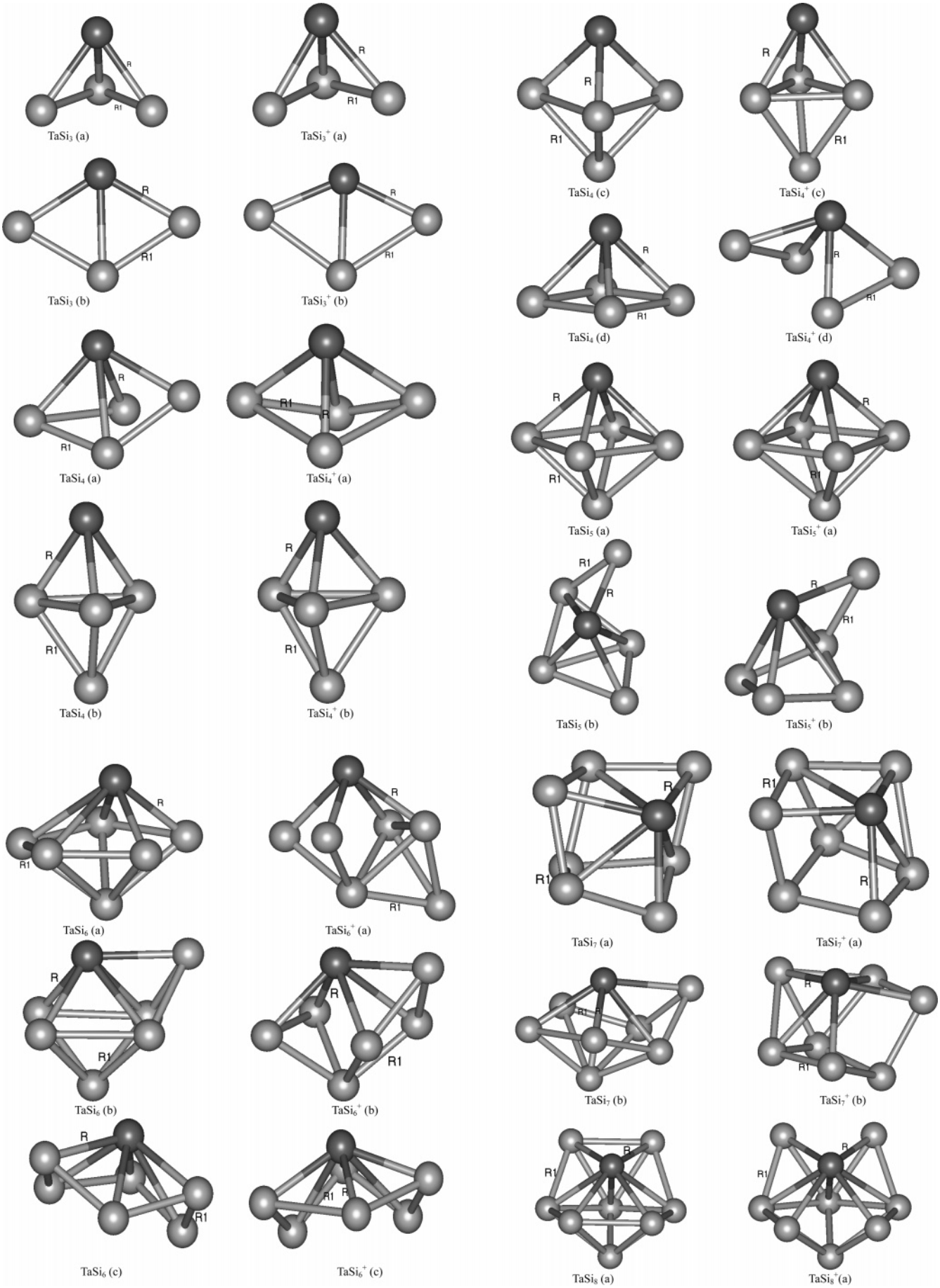
TaSi3 (a)
TaSi3+ (a)
TaSi4 (c)
TaSi4+ (c)
TaSi3 (b)
TaSi3+ (b)
TaSi4 (d)
TaSi4+ (d)
TaSi4 (a)
TaSi4+ (a)
TaSi5 (a)
TaSi5+ (a)
TaSi4 (b)
TaSi4+ (b)
TaSi5 (b)
TaSi5+ (b)
TaSi6 (a)
TaSi6+ (a)
TaSi7 (a)
TaSi7+ (a)
TaSi6 (b)
TaSi6+ (b)
TaSi7 (b)
TaSi7+ (b)
TaSi6 (c)
TaSi6+ (c)
TaSi8 (a)
TaSi8+ (a)

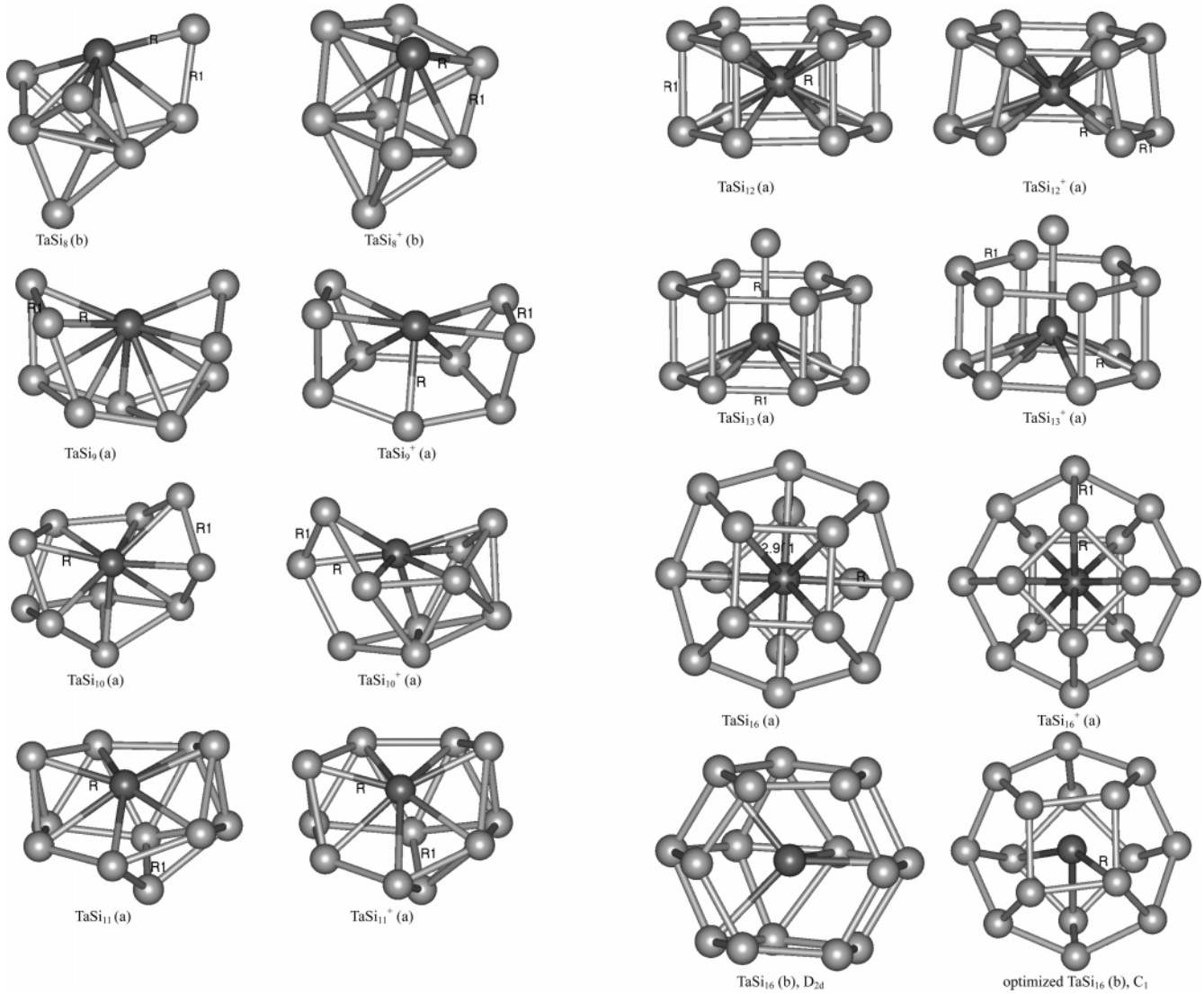

Figure 1. Equilibrium geometrics of $TaSi_n$ and $TaSi_n^+$ clusters ($n = 3-13, 16$).

$TaSi_3^+$. Two $TaSi_3^+$ isomers are considered (Figure 1). The optimized results show that the charged isomers maintain the geometrical frameworks that are analogous to the neutrals. Moreover, the 3a(+) isomer is more stable than the 3b(+) isomer. Furthermore, the shortest Ta−Si (at one side) and Si−Si bond lengths in the 3a(+) are slightly shorter than those in the corresponding neutral. It is worth pointing out that the HOMO−LUMO gap of the most stable 3a(+) structure is smaller than that of its neutral because of the different HOMO and LUMO compositions in the neutral and charged clusters. In the planar 3b(+) structure, all Si−Si bond lengths become longer while all the Ta−Si bond lengths are shortened, together with the 3b(+) cluster being more compressed in geometry, as compared to the neutral 3b cluster.

$TaSi_4^+$ According to the experimental results,[20] several competitive $TaSi_4^+$ isomers (4a(+), 4b(+), 4c(+), and 4d(+)) are investigated. As compared to the neutral 4a geometry, the serious deformed 4a(+) geometry is described as a bipyramidal structure with Ta atom being capped on the deformed rhombus; furthermore, the Ta−Si and Si−Si bond lengths are changed. In analogy to the 4b geometry, the C_{3v} 4b(+) structure is seen as a trigonal bipyramidal structure, and the 4b(+) is more stable than the 4a(+) isomer. The optimized 4c(+) is similar to the 4b(+) in geometry; however, the 4c(+) isomer is more stable than the 4b(+) isomer. It should be pointed out that the HOMO−LUMO gaps of the 4c(+) and the 4b(+) structures become larger than the corresponding neutral species, indicating that the two isomers have higher chemical stabilities than the neutrals. Finally, the square pyramidal C_{4v} 4d geometry is significantly distorted because of the positive charge, and the final stable C_1 4d(+) geometry has the framework that is analogous to the 4a(+).

For all of the $TaSi_4^+$ species, the energy order is 4c(+), 4b(+), 4a(+), and 4d(+); which is different from that of (4a, 4b, 4c, and 4d) species, reflecting that the 4c(+) structure is the most stable cationic structure among all of the investigated isomers and that the geometries and the energy orders of $TaSi_4^+$ clusters are influenced significantly by the positive charge.

$TaSi_5^+$. As seen from Figure 1, the charged 5a(+) structure, which corresponds to the lowest-energy structure and ground state, is distorted slightly into a low-symmetry structure as compared to the neutral 5a. The 5b(+) structure is described as an edge-capped triangle bipyramidal structure with the shortest Ta−Si and Si−Si bond lengths being shorter than those of the neutral 5b isomer. It should be mentioned that the HOMO−LUMO gaps of the two $TaSi_5^+$ structures also become quite smaller than the corresponding neutrals, reflecting that the $TaSi_5^+$ isomer has a decreased chemical stability.

$TaSi_6^+$. Three initial low-lying $TaSi_6^+$ structures, which are described as, respectively, the distorted pentagon bipyramidal

TABLE 2: Geometries, Total Bonding Energies (E_T), and Vibrational Frequencies (freq) of $TaSi_n$ and $TaSi_n^+$ Clusters at the Scalar Relativistic Level

cluster	isomer	sym	state	E_T (eV)	R (Å)	$R1$ (Å)	freq (cm^{-1})
TaSi	1a	$C_{\infty v}$	$^4\phi$	−5.7659	2.357		402.2
	1a(+)	$C_{\infty v}$	$^3\phi$	1.7253	2.380		418.2
$TaSi_2$	2a	C_s	$^4A''$	−11.6390	2.170		285.7
	2a(+)	C_s	$^3A''$	−4.3887	2.170		287.6
	2b	$D_{\infty h}$	Σ_u^{2-}	−8.7527	2.345		267.1
	2b(+)	$D_{\infty h}$	Σ_u^{1-}	−1.5943	2.346		
$TaSi_3$	3a	C_s	$^2A'$	−16.9345	2.364	2.548	116.1
	3a(+)	C_s	$^1A'$	−9.4121	2.362	2.450	190.4
	3b	C_{2v}	$^2B_2$	−15.8564	2.395	2.406	63.3
	3b(+)	C_{2v}	$^1A_1$	−8.7009	2.363	2.602	72.3
$TaSi_4$	4a	C_1	^2A	−21.5197	2.430	2.317	104.7
	4a(+)	C_1	^1A	−14.1522	2.432	2.288	86.3
	4b	C_{3v}	$^2A_1$	−21.4566	2.443	2.464	170.7
	4b(+)	C_{3v}	$^1A_1$	−15.1229	2.404	2.486	188.1
	4c	C_s	$^2A''$	−21.3960	2.402	2.426	80.1
	4c(+)	C_s	$^1A'$	−15.1282	2.398	2.485	80.8
	4d	C_{4v}	$^2B_1$	−20.5013	2.488	2.492	157.2
	4d(+)	C_2	^1A	−14.1343	2.424	2.451	61.0
$TaSi_5$	5a	C_{4v}	$^2B_1$	−26.8257	2.490	2.481	95.8
	5a(+)	C_1	^1A	−19.1371	2.447	2.426	72.9
	5b	C_1	^2A	−26.2688	2.451	2.318	70.0
	5b(+)	C_1	^1A	−19.0287	2.496	2.260	20.7
$TaSi_6$	6a	C_1	^2A	−31.4186	2.430	2.350	55.4
	6a(+)	C_1	^1A	−24.9559	2.459	2.389	126.7
	6b	C_1	^2A	−31.1976	2.460	2.444	105.7
	6b(+)	C_1	^1A	−24.2226	2.469	2.398	93.6
	6c	C_s	$^2A'$	−31.0421	2.524	2.323	95.7
	6c(+)	C_1	^1A	−23.8843	2.457	2.288	77.3
$TaSi_7$	7a	C_1	^2A	−36.4944	2.459	2.345	48.5
	7a(+)	C_1	^1A	−29.7305	2.505	2.328	68.9
	7b	C_1	^2A	−36.4080	2.528	2.346	54.0
	7b(+)	C_1	^1A	−29.7310	2.507	2.322	66.9
$TaSi_8$	8a	C_2	^2B	−41.4098	2.558	2.484	79.2
	8a(+)	C_2	^1A	−34.4150	2.572	2.423	75.2
	8b	C_s	$^2A'$	−40.3773	2.511	2.496	45.2
	8b(+)	C_1	^1A	−34.4385	2.308	2.329	91.9
$TaSi_9$	9a	C_1	^2A	−45.0098	2.556	2.332	32.3
	9a(+)	C_1	^1A	−38.2335	2.555	2.320	5.1
$TaSi_{10}$	10a	C_1	^2A	−50.3240	2.584	2.282	23.8
	10a(+)	C_1	^1A	−43.4522	2.563	2.330	34.7
$TaSi_{11}$	11a	C_1	^2A	−55.5925	2.533	2.384	61.1
	11a(+)	C_1	^1A	−48.4812	2.519	2.375	42.6
$TaSi_{12}$	12a	D_{6h}	$^2A_{2u}$	−60.9541	2.714	2.412	4.84
	12a(+)	C_1	^1A	−53.8188	2.599	2.334	30.3
$TaSi_{13}$	13a	C_{2v}	$^2A_2$	−65.3763	2.531	2.421	68.7
	13a(+)	C_{2v}	$^1A_1$	−59.1468	2.663	2.427	79.7
$TaSi_{16}$	16a	C_{4v}	$^2B_1$	−80.7723	2.782	2.291	20.8
	16a(+)	C_{4v}	$^1A_1$	−74.9159	2.803	2.301	74.4
	16b	C_1	^2A	−80.7765	2.874		
	16b(+)	C_1	^1A	−74.7950			

6a+ and the capped quadrangle bipyramidalal 6b+ as well as the distorted hexagon pyramidal 6c+, are considered. After geometry optimization, a large deviation of geometry occurs to the 6a(+) structure; furthermore, the large variation of geometry leads to a difference of 1.13 eV between the calculated AIP (6.46 eV) and VIP (7.59 eV) of the 6a isomer. In addition, the HOMO−LUMO gap of the 6a(+) structure is larger than those of the 6b(+) and 6c(+) species. As compared to the neutral geometry (6b), the shortest Ta−Si bond length of the 6b(+) structure becomes longer while the shortest Si−Si bond length is shortened, and the total bonding energy of the 6b(+) is higher than the 6a(+) isomer by 0.733 eV. Finally, the optimized 6c-(+) geometry is also obviously higher in total bonding energy than the 6a(+) isomer, reflecting that it is less stable than the 6a(+) isomer. On the basis of calculated total bonding energy of the 6a(+), 6b(+), and 6c(+) isomers, one finds that the 6a-(+) isomer is the lowest-energy structure and the ground state; the corresponding electronic state is predicted to be ^1A.

$TaSi_n^+$(n = 7−13). For the $TaSi^+_7$ clusters, the distorted cube 7a(+) and capped pentagon bipyramidal 7b(+) are considered. The optimized 7a(+) geometry is similar to the 7b(+) geometry; however, the 7a(+) is less stable than 7b(+) because the 7b-(+) isomer is slightly lower in total bonding energy than the 7a(+) isomer, by 0.005 eV. Furthermore, the HOMO−LUMO gaps of the 7a(+) (1.387 eV) and 7b(+) (1.398 eV) isomers become quite bigger as compared to the corresponding neutrals. As for the $TaSi_8^+$ clusters, the optimized 8a(+) geometry deviates slightly to the neutral geometry while the charged 8b-(+) geometry is the large rearrangement of the neutral 8b geometry. Furthermore, the 8b(+) geometry can be described as one Si atom being capped on the most stable 7b(+), and its total bonding energy is lower than that of the 8a(+) isomer by 0.0235 eV; Consequently, the 8b(+) structure is the most stable $TaSi_8^+$ isomer and ground state; the corresponding electronic state is labeled as having ^1A character. On the basis of the discussions above and calculated results shown in Table 2, it apparently reveals that the positive charge significantly influences the geometries and stabilities of the charged $TaSi_7^+$ and $TaSi_8^+$ clusters. As for as the investigated $TaSi_n^+$ ($n = 9-13$) clusters, except for $TaSi_{13}^+$ cluster, the Ta−Si bond lengths in the $TaSi_n^+$ ($n = 9-12$) become slightly shorter than those in the corresponding neutral forms.

$TaSi_{16}^+$. Two initial isomers (Figure 1), namely, the cationic 16a and 16b, are investigated. The cagelike 16a and 16a(+) clusters with C_{4v} symmetry are the stable structures. Furthermore, the 16a(+) isomer has a HOMO−LUMO gap of 1.734 eV, which can be detected by experimental methods and is smaller than that (1.9 eV) of the $TiSi_{16}$ clusters.[1] The unstable D_{2d} 16b isomer is a Frank−Kasper (FK) polyhedral structure.[2] After a relaxation of the geometry, the C_1 16b structure is optimized to be a stable structure, which is similar to the 16a framework and the most stable neutral C_1 isomer is slightly lower in total bonding energy than the 16a C_{4v} isomer. However, the most stable C_{4v} $TaSi_{16}^+$ geometry is a fullerene-like structure with electronic state of $^1A_1$.

Generally, the $TaSi_n^+$ ($n = 1-3$, 5, 9−13) clusters keep the same energy orders as the neutral $TaSi_n$ clusters; However, the $TaSi_4^+$($n = 4$, 6−8) isomers have large deviations of the neutral geometries. Theoretical results indicate that the influences of the positive charge on the electronic properties of the medium-sized $TaSi_n$ ($n = 3-12$) clusters are significantly larger than those of the large-sized ones. All of these findings prove the prediction in the previous neutral $TaSi_n$ ($n = 1-13$).[32]

3.2. Fragmentation Energies. To compare the relative stabilities of the $TaSi_n^+$ ($n = 1-13$) clusters with the experimental mass spectra measurements, it is significant to calculate the fragmentation energies ($D(n, n-1)$) of the most stable $TaSi_n^+$($n = 1-13$) clusters. The fragmentation energies of the most stable $TaSi_n^+$ ($n = 1-13$) clusters are defined as

$$D(n, n-1) = E_T(TaSi_{n-1}^+) + E_T(Si) - E_T(TaSi_n^+)$$

where $E_T(TaSi_{n-1}^+)$, $E_T(Si)$, $E_T(Ta^+)$, and $E_T(TaSi_n^+)$ denote the total bonding energies of the most stable $TaSi_{n-1}^+$, Si atom, Ta^+, and $TaSi_n^+$ clusters, respectively. The calculated results are plotted as the curves of the $D(n, n-1)$ against the corresponding number of the Si atoms. The features of the size-evolution are intuitively shown in Figure 2, and the peaks of the curves correspond to the clusters having enhanced local stabilities.

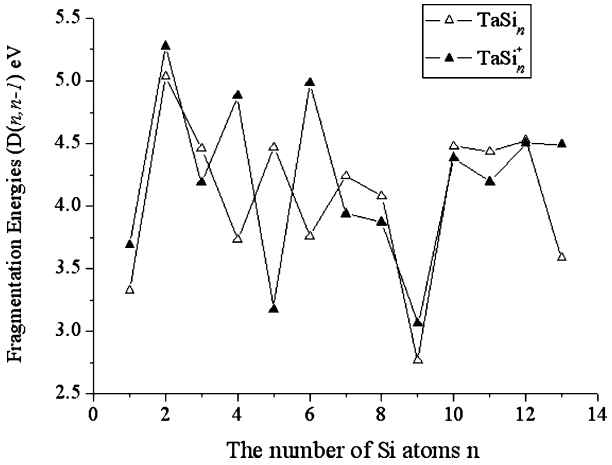

Figure 2. Size dependence of the fragmentation energies of $TaSi_n$ and $TaSi_n^+$ clusters.

As seen from Figure 2, the fragmentation energies of the $TaSi_n^+$ clusters display that some stable structures are found at $n = 2, 4, 6, 8, 10-13$, which are different from those of the neutrals with $n = 2, 5, 7, 10-12$;[32] indicating that the corresponding clusters are relatively more stable than their neighboring clusters. According to the calculated fragmentations energies of the charged $TaSi_n^+$ clusters, one finds that the large deviations of the fragmentation energies are exhibited at the medium-sized neutral and charged $TaSi_n$ ($n = 4-8$) clusters and $TaSi_{13}$ (and $TaSi_{13}^+$), reflecting that the positive charge in the medium-sized $TaSi_n^+$ plays an important role in the relative stabilities. Furthermore, the theoretical results reveal that the calculated abundant $TaSi_n^+$($n = 4, 6, 8, 11-13$) clusters are in agreement with the recent experimental measurements of the abundant $TaSi_n^+$ ($n = 4, 6, 8, 9, 11, 12$) clusters.[20]

3.3. Adiabatic Ionization Potentials and Vertical Ionization Potentials. We have calculated the AIPs and VIPs, which are defined as the difference of total bonding energies in the following ways:

$$\mathrm{AIP} = E\ (\text{optimized } TaSi_n^+) - E\ (\text{optimized } TaSi_n)$$

$$\mathrm{VIP} = E\ (TaSi_n^+ \text{ with neural geometry}) - E\ (\text{optimized } TaSi_n)$$

It should be mentioned that the AIPs correspond to the bonding energy gaps between the lowest-energy $TaSi_n$ and $TaSi_n^+$ clusters. As seen from Table 3, there are always some differences between the AIP and corresponding VIP values for the $TaSi_n$ clusters, reflecting that the geometric rearrangements happen from the neutrals to the cationic clusters. The two curves in Figure 3 represent the size dependence of the AIP and VIP for the lowest-energy $TaSi_n$ clusters, the VIPs of the $TaSi_n$ ($n = 4, 6-13$) exceed the corresponding AIPs; particularly, the remarkable VIPs of the $TaSi_n$ ($n = 4$ and $n = 6$) are lower by approximately 0.7 eV and 1.1 eV than the AIPs, respectively; indicating that the positive charge results in the considerable geometric rearrangements of the medium-sized $TaSi_n$ (4, 6−13) clusters, and that their cationic clusters are easily generated experimentally and correspond to the abundant peaks in mass spectroscopy, which are in good agreement with experimental observations and discussions above.[20]

3.4. HOMO−LUMO Gaps. The HOMO and LUMO energies of the $TaSi_n^+$ clusters are lower than those of the corresponding $TaSi_n$, and the HOMO−LUMO gaps of the $TaSi_n^+$ clusters are bigger than those of the neutral ones except

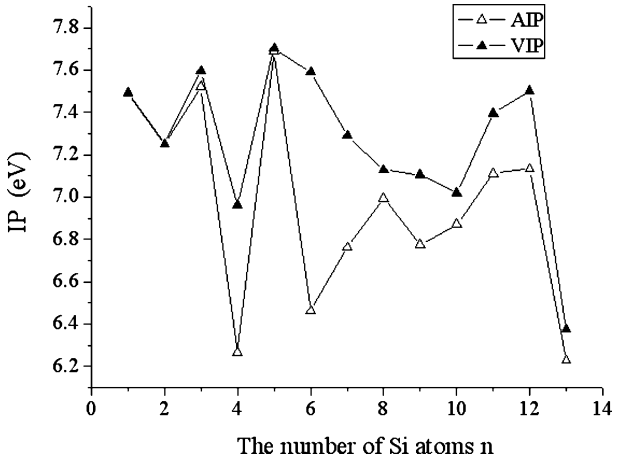

Figure 3. Size dependence of vertical ionization potentials and adiabatic ionization potentials of $TaSi_n$ clusters.

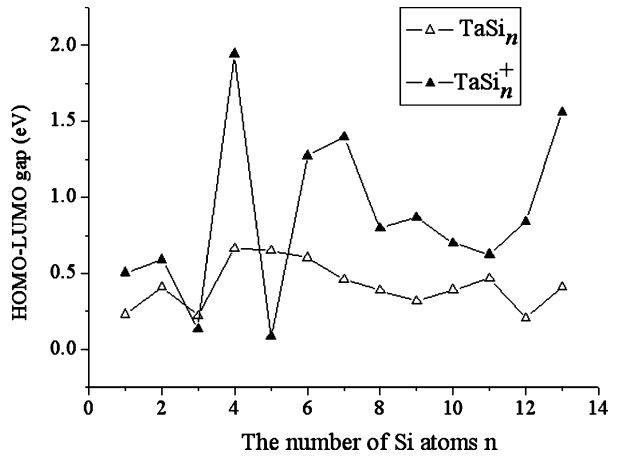

Figure 4. Size dependence of the HOMO−LUMO gaps of $TaSi_n$ and $TaSi_n^+$ clusters.

TABLE 3: AIPs and VIPs of $TaSi_n$ Clusters as Well as the Net Mulliken Population (MP) and Hirshfeld Charge (HC) of the Ta Atom

cluster	isomer	AIP (eV)	VIP (eV)	MP	HC	MP(+)	HC(+)
TaSi	1a	7.4912	7.4950	0.0834	0.1332	0.5906	0.6847
$TaSi_2$	2a	7.2503	7.2515	0.1167	0.1545	0.5210	0.6282
$TaSi_3$	3a	7.1579	7.1576	0.0867	0.1902	0.3428	0.4832
	3b	7.5224	7.5965	0.2110	0.2404	0.3847	0.4371
$TaSi_4$	4a	7.1555	7.1554	0.1605	0.2517	0.3518	0.4902
	4b	7.3675	7.4467	0.0965	0.2299	0.3694	0.5019
	4c	6.3337	6.4266	0.1103	0.2011	0.3715	0.5034
	4d	6.2678	6.9643	0.1141	0.2340	0.1856	0.3311
$TaSi_5$	5a	6.3760	6.8074	0.1288	0.2202	0.1897	0.4304
	5b	7.6886	7.7035	0.2086	0.2391	0.3349	0.4211
$TaSi_6$	6a	6.4627	7.5916	0.1646	0.2618	0.3085	0.3739
	6b	6.9750	7.1121	0.1788	0.2045	0.2842	0.3443
	6c	7.2401	7.4257	0.1863	0.2032	0.1996	0.2894
$TaSi_7$	7a	7.1597	7.4972	0.1814	0.2170	0.2230	0.3166
	7b	6.7639	7.2914	0.1657	0.2268	0.2236	0.3174
$TaSi_8$	8a	6.6770	6.4928	0.1557	0.1631	0.1901	0.2500
	8b	6.9948	7.1288	0.2464	0.1688	0.2630	0.3403
$TaSi_9$	9a	5.9388	7.1901	0.2979	0.0884	0.2156	0.1415
$TaSi_{10}$	10a	6.7763	7.1070	0.2425	0.0290	0.2470	0.0747
$TaSi_{11}$	11a	6.8718	7.0193	0.2678	0.0551	0.2227	0.1175
$TaSi_{12}$	12a	7.1114	7.3954	0.0016	−0.0193	−0.1176	0.0013
$TaSi_{13}$	13a	7.1353	7.5029	−0.0429	−0.1071	−0.0905	−0.0573
$TaSi_{16}$	16a	6.2295	6.3761	−0.1401	0.0275	−0.1993	0.0148
	16b	5.9815	5.8564	−0.1146	0.0298	−0.1905	0.0153

for the three isomers: $TaSi_3^+$(3a), $TaSi_4^+$(4a), and $TaSi_5^+$(5a) (Table 3 and Figure 4). These findings suggest that the chemical stability of the $TaSi_n^+$ clusters is improved in comparison with the $TaSi_n$ isomers. In the other words, the positive charge in

TABLE 4: HOMO and LUMO Energies as Well as the HOMO− LUMO Gaps of $TaSi_n$ and $TaSi_n^+$ Clusters

cluster	isomer	HOMO	LUMO	gap	HOMO (+)	LUMO (+)	gap (+)
TaSi	1a	−4.4267	−4.1979	0.2288	−10.8109	−10.3069	0.5040
$TaSi_2$	2a	−4.5424	−4.1367	0.4057	−10.4864	−9.8963	0.5901
$TaSi_3$	3a	−4.6409	−4.4205	0.2204	−10.0699	−9.9357	0.1342
	3b	−4.9445	−4.5074	0.4371	−10.0043	−9.2776	0.7267
$TaSi_4$	4a	−5.0150	−4.3501	0.6649	−10.0212	−9.6608	0.3604
	4b	−4.2105	−3.7879	0.4226	−10.3782	−8.4314	1.9468
	4c	−4.6860	−4.1017	0.5843	−10.3800	−8.4342	1.9458
	4d	−4.5250	−4.3768	0.1482	−9.6015	−9.2498	0.3537
$TaSi_5$	5a	−5.3829	−4.7335	0.6494	−9.8718	−9.7895	0.0823
	5b	−5.1249	−4.6003	0.5246	−9.7183	−9.2112	0.5071
$TaSi_6$	6a	−5.4224	−4.8184	0.6040	−9.6522	−8.3775	1.2747
	6b	−4.9563	−4.4723	0.4840	−9.6674	−8.9751	0.6923
	6c	−5.2108	−4.7579	0.4529	−9.6751	−8.7905	0.8846
$TaSi_7$	7a	−5.1310	−4.6738	0.4572	−9.6497	−8.2629	1.3868
	7b	−5.1828	−4.8741	0.3087	−9.6622	−8.2644	1.3978
$TaSi_8$	8a	−5.1219	−4.7365	0.3854	−9.5842	−8.7871	0.7971
	8b	−5.2478	−4.7606	0.4872	−9.2046	−7.7879	1.4167
$TaSi_9$	9a	−5.1869	−4.8716	0.3153	−9.1123	−8.2451	0.8672
$TaSi_{10}$	10a	−5.1316	−4.7408	0.3908	−9.2238	−8.5240	0.6998
$TaSi_{11}$	11a	−5.5224	−5.0564	0.4660	−9.2121	−8.5881	0.6240
$TaSi_{12}$	12a	−5.8587	−5.6557	0.2030	−9.2381	−8.3958	0.8421
$TaSi_{13}$	13a	−4.6650	−4.2571	0.4079	−9.4331	−7.8755	1.5576
$TaSi_{16}$	16a	−4.4694	−4.2880	0.1814	−9.3050	−7.5709	1.7341
	16b	−4.4810	−4.3502	0.1308	−9.3700	−7.5776	1.7924

most of the $TaSi_n^+$ clusters leads to the large HOMO−LUMO gaps so that these clusters become more chemically stable, making them attractive for cluster-assembled materials. On the basis of the discussions above, it is found that the charged clusters are more stable than the neutrals.

To explain why the HOMO−LUMO gaps of the charged clusters become smaller, we analyzed the orbital percentage compositions of the symmetrized fragment orbitals (SFO) of the HOMO and LUMO. The HOMO−LUMO gaps of the $TaSi_3^+$(3a), $TaSi_4^+$(4a), and $TaSi_5^+$(5a) clusters are decreased because the lower-energy s orbitals make more contributions to the LUMO of the charged clusters than that of the corresponding neutrals. In addition, it is easily found from the orbital percentage compositions that the d orbitals of the Ta atom and the p orbitals of Si atoms have equivalent proportions in HOMO and LUMO of the small-sized clusters; however, as the cluster size increases, the p orbitals of Si atoms become the dominate components of the HOMO and LUMO while the contribution of d orbitals of the Ta atom to HOMO−LUMO decreases gradually, exhibiting that the d orbitals of the encapsulated Ta atom in the charged and neutral clusters are saturated by the silicon bonds. It should be pointed out that the chemical activity of the neutral and charged $TaSi_n$ is decreased gradually as n goes from $n = 1$ to $n = 13$. This interesting finding is verified by recent experimental results of the chemical reactions among the H_2O and transition-metal silicon clusters.[1]

3.5. Population Analysis of the Ta Atom. The net MP and the corresponding HC values for the $TaSi_n$ and $TaSi_n^+$ clusters are positive for $n = 1-11$ (Table 3), suggesting that the charges transfer from the Ta to the Si_n ($n = 1-11$), which is different from the larger-sized clusters ($n > 11$). A disaccord between the MP and HC values happens when $n = 12$, the MP is positive while the HC is negative for the neutral $TaSi_{12}$ cluster; the situation is reverse for the charged $TaSi_{12}^+$. These findings show that the $TaSi_{12}$ or $TaSi_{12}^+$ is a turning point of the charge transfer. In fact, the phenomena is shown by the MP and HC values as the cluster size varies gradually from $n = 1$ to $n = 11$. The MP and HC are negative for the $TaSi_{13}$ and $TaSi_{13}^+$, and the MP are negative for the 16a and 16a(+); however, the corresponding HC values are positive.

In addition, according to the previous investigations on the transition-metal silicon clusters, one finds that if the charge transfers from the transition-metal atom to the Si atoms, the $TMSi_n$ have the small HOMO−LUMO gaps;[24−25,32] on the contrary, the $TMSi_n$ clusters with charges transferring from the Si atoms to the transition metal have large HOMO−LUMO gaps.[15,23,33]

4. Conclusions

The geometries, stabilities, and electronic properties of the $TaSi_n^+$ ($n = 1-13$, 16) clusters are investigated systematically by using the relativistic density functional method with generalized gradient approximation considering the exchange-correlation energy. The influence of the additional charge is discussed in detail and it is found that (1) The small-sized $TaSi_n^+$ structures keep frameworks basically analogous to those of the neutral $TaSi_n$ clusters while the medium- or large-sized charged clusters deform the neutral geometries because of the additional charges; particularly, the marked geometrical deformations are exhibited by the $TaSi_n^+$($n = 4, 6-8$) units, which are consistent with the pronounced differences between the corresponding VIPs and AIPs. (2) The fragmentation energies of the medium-sized $TaSi_n^+$ ($n = 4-8$, 13) clusters deviate to the calculated results of the neutral isomers; furthermore, the calculated relative stabilities are in good agreement with available experimental measurements.[20] (3) The HOMO−LUMO gaps of the $TaSi_n^+$ clusters are increased as compared to the neutral, indicating that the chemical stabilities of the $TaSi_n^+$ clusters have been proved to be enhanced simultaneously relative to the neutrals, especially obvious for $n = 4$, 6, and 7 clusters, making them attractive for cluster-assembled materials. (4) The contribution of d orbitals of Ta atom in the neutral and charged clusters to the HOMO and LUMO decreases gradually as the number of silicon atoms goes from $n = 1$ to $n = 13$, which are verified by recent experimental observation on the reactive activities between the H_2O and TM encapsulated Si_n cluster.[1] (5) The net Mulliken and Hirsheld populations of the tantalum atom in the $TaSi_n^+$ ($n = 1-11$) clusters are discussed and analyzed, finding that the turning point of charge transfer localizes at $n = 12$, which is the same as the neutral clusters. Furthermore, the positive charge

of the Ta atom in the most stable $TaSi_n^+$ clusters is decreased as the size of the clusters increases. In the other words, the additional charge in the small-sized $TaSi_n^+$ clusters distributes mainly on the Ta atom; however, the extra charge in the medium-sized and large-sized charged clusters contributes on the Si_n frame of $TaSi_n^+$ clusters. (6) Finally, the most stable $TaSi_{16}^+$ cluster with a slight distorted C_{4v} symmetry is found to be a cagelike structure. Furthermore, the charged $TaSi_{16}^+$ cluster with a HOMO−LUMO gap of 1.734 eV is experimentally detectable and can be exploited for device applications.

Acknowledgment. P.G. thanks Prof. Wen Zhenyi for his significant discussions. This work is supported by National Natural Science Foundation of China (cooperation item of west and east, Grant No. 10247007); Natural Science Foundation of ShaanXi province (Grant No. 2002A09); Special Item Foundation of Educational Committee of ShaanXi province (Grant No. 02JK050); and National Natural Science Foundation of P. R. China (20173055, 90206033).

References and Notes

(1) Koyasu, K.; Akutsu, M.; Mitsui, M.; Nakajima, A. *J. Am. Chem. Soc*. **2005**, *127*, 4998.
(2) Jarrold, M. F. *Science* **1991**, *252*, 1085.
(3) Bloomfield, L. A.; Freeman, R. R.; Brown, W. L. *Phys. Rev. Lett*. **1985**, *54*, 2246.
(4) Li S.; Van Zee, R. J.; Weltner, W., Jr.; Raghavachari, K. *Chem. Phys. Lett*. **1995**, *243*, 275.
(5) Han, J. G.; Hagelberg, F. *Comput. Lett.* **2005**, *1*, 230.
(6) Raghavachari, K.; Rohlfing, C. M. *J. Chem. Phys*. **1986**, *84*, 5673.
(7) Raghavachari, K.; Rohlfing, C. M. *J. Chem. Phys*. **1988**, *89*, 2219.
(8) Kaxiras, E.; Jackson, K. *Phys. Rev. Lett*. **1993**, *71*, 727.
(9) Rothlisberger, U.; Andreoni, W.; Parrinello, M. *Phys. Rev. Lett*. **1994**, *72*, 665.
(10) Ho, K. M.; Shvartsburg, A. A.; Pan, B.; Lu Z. Y.; Wang, C. Z.; Wacker, J. G.; Fye, J.; Jarrold, M. F. *Nature* **1998**, *392*, 582.
(11) Hagelberg, F.; Leszczynski, J.; Murashov, V. *THEOCHEM* **1998**, *454*, 209.
(12) Rata, I.; Shvartsburg, A. A.; Horoi, M.; Frauenheim, T.; Siu, K. W. M.; Jackson, K. A. *Phys. Rev. Lett.* **2000**, *85*, 546.
(13) Kumar, V.; Kawazoe, Y. *Phys. Rev. Lett*. **2001**, *87*, 045503.
(14) Zhao, R. N.; Ren, Z. Y.; Guo, P.; Bai, J. T.; Zhang, C. H.; Han, J. G. *J. Phys. Chem. A.* **2006**, *110*, 4071.
(15) Kumar, V.; Kawazoe, Y. *Phys. Rev. B* **2002**, *65*, 073404.
(16) Wang J.; Han J. G. *J. Chem. Phys.* **2005**, *123*, 64306.
(17) Singh, A. K.; Briere T. M.; Kumar, V.; Kawazoe, Y. *Phys. Rev. Lett*. **2003**, *91*, 146802.
(18) Beck, S. M. *J. Chem. Phys*. **1987**, *87*, 4233.
(19) Beck, S. M. *J. Chem. Phys*. **1989**, *90*, 6306.
(20) Hiura, H.; Miyazaki, T.; Kanayama, T. *Phys. Rev. Lett*. **2001**, *86*, 1733.
(21) Han, J. G.; Hagelberg F. *THEOCHEM* **2001**, *549*, 165.
(22) Han, J. G.; Hagelberg F. *Chem. Phys*. **2001**, *263*, 255.
(23) Han, J. G.; Shi, Y. Y. *Chem. Phys.* **2001**, *266*, 33.
(24) Xiao, C.; Hagelberg, F.; Ovcharenko, I.; Lester, W. A., Jr. *THEOCHEM* **2001**, *549*, 181.
(25) Xiao, C.; Hagelberg, F.; Lester, W. A., Jr. *Phys. Rev. B* **2002**, *66*, 075425.
(26) Khanna, S. N.; Rao, B. K.; Jena, P. *Phys. Rev. Lett.* **2002**, *89*, 016803.
(27) Han, J. G. *Chem. Phys*. **2003**, *286*, 181.
(28) Gueorguiev, G. K.; Pacheco, J. M. *J. Chem. Phys.* **2003**, *119*, 10313.
(29) Lu, J.; Nagase, S. *Phys. Rev. Lett* **2003**, *90*, 115506.
(30) Sen, P.; Mitas, L. *Phys. Rev. B* **2003**, *68*, 155404.
(31) Han, J. G.; Ren, Z. Y.; Lu, B. Z. *J. Phys. Chem. A* **2004**, *108*, 5100.
(32) Guo, P.; Ren, Z. Y.; Wang, F.; Bian, J.; Han, J. G.; Wang, G. H. *J. Chem. Phys*. **2004**, *121*, 12265.
(33) Kawamura, H.; Kumer, V.; Kawazoe, Y. *Phys. Rev. B* **2004**, *70*, 245433.
(34) Ren, Z. Y.; Li, F.; Guo, P.; Han, J. G. *THEOCHEM* **2005**, *718*, 165.
(35) Jia, L. C. et al., submitted for publication.
(36) Wang, J.; Han, J. G. *J. Phys. Chem. B* **2006**, *110*, 7820.
(37) van Lenthee, E.; Bearends, E. J.; Snijders, J. G. *J. Chem. Phys.* **1994**, *101*, 9783.
(38) van Lenthee, E.; Snijders, J. G.; Bearends, E. J. *J. Chem. Phys*. **1996**, *105*, 6505.
(39) Velde, G. Te; Baerends, E. J. *J. Comput. Phys*. **1992**, *99*, 84.
(40) Vosko, S. H.; Wilk, L.; Nusair, M. *Can. J. Phys*. **1980**, *58*, 1200.
(41) Becke, A. D. *Phys. Rev. A* **1988**, *38*, 2398.
(42) Perdew, J. P.; Wang, Y. *Phys. Rev. B* **1986**, *33*, 8822.
(43) Huber, K. P.; Herzberg, G. *Constants of Diatomic Molecules*; Van Nostrand Reinhold: New York, 1979.
(44) Chatillon, C.; Aillbert, M.; Pattoret, A.; Acad, C. R. *Sci. Ser*. **1975**, *C 280*, 1505
(45) Honea, E. C.; Ogura, A.; Peale, D. R.; Félix, C.; Murray, C. A.; Raghavachari, K.; Sprenger, W. O.; Jarrold, M. F.; Brown, W. L. *J. Chem. Phys*. **1999**, *110*, 12161
(46) (a) Huaiming, W.; Craig, R.; Haouari, H.; Dong, J. G.; Hu, Z. D.; Vivoni, A.; Lombardi, J. R.; Lindsay, D. M. *J. Chem. Phys*. **1995**, *103*, 3289. (b) Bérces, A. *Spectrochim. Acta, Part A* **1997**, *53*, 1257.
(47) Majumdar, D.; Balasubramanian, K. *Chem. Phys. Lett.* **1998**, *284*, 273.